Bis(diphenylphosphino)methane Dioxide Complexes of Lanthanide Trichlorides: Synthesis, Structures and Spectroscopy [†]

Robert D. Bannister [ID]**, William Levason** [ID] **and Gillian Reid *** [ID]

School of Chemistry, University of Southampton, Southampton SO17 1BJ, UK;
r.d.bannister@soton.ac.uk (R.D.B.); wxl@soton.ac.uk (W.L.)
* Correspondence: gr@soton.ac.uk
† Dedicated to Dr. Howard Flack (1943–2017).

check for updates

Abstract: Bis(diphenylphosphino)methane dioxide ($dppmO_2$) forms eight-coordinate cations $[M(dppmO_2)_4]Cl_3$ (M = La, Ce, Pr, Nd, Sm, Eu, Gd) on reaction in a 4:1 molar ratio with the appropriate $LnCl_3$ in ethanol. Similar reaction in a 3:1 ratio produced seven-coordinate $[M(dppmO_2)_3Cl]Cl_2$ (M = Sm, Eu, Gd, Tb, Dy, Ho, Er, Tm, Yb), whilst $LuCl_3$ alone produced six-coordinate $[Lu(dppmO_2)_2Cl_2]Cl$. The complexes have been characterised by IR, ^{1}H and ^{31}P{^{1}H}-NMR spectroscopy. X-ray structures show that $[M(dppmO_2)_4]Cl_3$ (M = Ce, Sm, Gd) contain square antiprismatic cations, whilst $[M(dppmO_2)_3Cl]Cl_2$ (M = Yb, Dy, Lu) have distorted pentagonal bipyramidal structures with apical Cl. The $[Lu(dppmO_2)_2Cl_2]Cl$ has a *cis* octahedral cation. The structure of $[Yb(dppmO_2)_3(H_2O)]Cl_3 \cdot dppmO_2$ is also reported. The change in coordination numbers and geometry along the series is driven by the decreasing lanthanide cation radii, but the chloride counter anions also play a role.

Keywords: lanthanide trichloride complexes; diphosphine dioxide; coordination complexes; X-ray structures

1. Introduction

Early work viewed the chemistry of the lanthanides (Ln) (Ln = La–Lu, ≠ Pm unless otherwise indicated) in oxidation state III as very similar and often only two or three elements were examined, and the results were assumed to apply to all. More recent work has shown this to be a very unreliable approach and detailed studies of all fourteen elements (excluding only the radioactive Pm) are required to establish properties and trends [1,2]. Sometimes yttrium is also included since it is similar in size to holmium. The main changes along the series are due to the lanthanide contraction, the reduction in the radius of the M^{3+} ions between La (1.22 Å) and Lu (0.85 Å), and at some point a reduction in coordination number may be driven by steric effects, especially with bulky ligands. However, the decrease in radius also results in an increase in the charge/radius ratio along the series and this can lead to significant electronic effects on the ligand preferences. This interplay of steric and electronic effects means that changes in coordination number or ligand donor set can occur at different points along the series with different ligands. The effects are very nicely demonstrated in a recent article, which examined the changes which occurred in the series of lanthanide nitrates with complexes of 2,2′-bipyridyl, 2,4,6-tri-α-pyridyl-1,3,5-triazine and 2,2′; 6′,2″-terpyridine [2]. Tertiary phosphine oxides have proved popular ligands to explore lanthanide chemistry and the area has been the subject of a comprehensive review [3], and several detailed studies of trends along the series La-Lu have been reported [4–7]. We reported bis(diphenylphosphino)methane dioxide ($dppmO_2$) formed square-antiprismatic

cations $[La(dppmO_2)_4]^{3+}$ with Cl, I or $[PF_6]$ counter ions, but lutetium gave only octahedral $[Lu(dppmO_2)_2X_2]^+$ (X = Cl, I) and $[Lu(dppmO_2)_2Cl(H_2O)]^{2+}$ [8]. Other dppmO$_2$ complexes reported include several types with $Ln(NO_3)_3$ [4], $[Dy(dppmO_2)_4][CF_3SO_3]_3$ [9], $[Eu(dppmO_2)_4][ClO_4]_3$ [10], $[La(dppmO_2)_4][CF_3SO_3]_3$ and $[Lu(dppmO_2)_3(H_2O)][CF_3SO_3]_3$ [11]. Here, we report a systematic study of the systems LnCl$_3$-dppmO$_2$ for all fourteen accessible lanthanides.

2. Materials and Methods

Infrared spectra were recorded as Nujol mulls between CsI plates using a Perkin-Elmer Spectrum 100 spectrometer over the range 4000–200 cm^{-1}. ^{1}H and ^{31}P{^{1}H}-NMR spectra were recorded using a Bruker AV–II 400 spectrometer and are referenced to the protio resonance of the solvent and 85% H$_3$PO$_4$, respectively. Microanalyses were undertaken by London Metropolitan University or Medac. Hydrated lanthanide trichlorides and anhydrous LnCl$_3$ (Ln–Nd, Pr, Gd, Ho) were from Sigma-Aldrich and used as received. The Ph$_2$PCH$_2$PPh$_2$ (Sigma-Aldrich) in anhydrous CH$_2$Cl$_2$ was converted to Ph$_2$P(O)CH$_2$P(O)Ph$_2$ by air oxidation catalysed by SnI$_4$ [12].

X-Ray Experimental. Details of the crystallographic data collection and refinement parameters are given in Table 1. Many attempts were made to grow crystals for X-ray examination from a variety of solvents including EtOH and CH$_2$Cl$_2$, either by slow evaporation or layering with hexane or pentane. The crystal quality was often rather poor, and all of the structures have disordered co-solvent, either water or ethanol. No attempt was made to locate the protons on the co-solvent. Several showed disorder in one or more of the phenyl rings. Good-quality crystals used for single crystal X-ray analysis were grown from $[Lu(dppmO_2)_4\}Cl_2]Cl$ (CH$_2$Cl$_2$/hexane), $[Ce(dppmO_2)_4]Cl_3$, $[Sm(dppmO_2)_4]Cl_3$, $[Gd(dppmO_2)_4]Cl_3$ (EtOH), $[Yb(dppmO_2)_3Cl]Cl_2$, $[Yb(dppmO_2)_3(H_2O)]Cl_3$·dppmO$_2$ (EtOH), $[Lu(dppmO_2)_3Cl]Cl_2$ (CH$_2$Cl$_2$).

Data collections used a Rigaku AFC12 goniometer equipped with a HyPix-600HE detector mounted at the window of an FR-E+ SuperBright molybdenum (λ = 0.71073 Å) rotating anode generator with VHF Varimax optics (70 µm focus) with the crystal held at 100 K (N$_2$ cryostream). Structure solution and refinements were performed with either SHELX(S/L)97 or SHELX(S/L)2013 [13,14]. The crystallographic data in cif format have been deposited as CCDC 2033611-2033618.

All samples were dried in high vacuum at room temperature for several hours, but this treatment does not remove lattice water or alcohol. Heating the samples in vacuo is likely to cause some decomposition of the complexes [7] and was not applied.

$[La(dppmO_2)_4]Cl_3$·4H$_2$O and $[Lu(dppmO_2)_2Cl_2]Cl$·H$_2$O were made as described [8]. The individual new complexes were isolated as described below, with yields of 50–80%.

$[Ce(dppmO_2)_4]Cl_3$·6H$_2$O—CeCl$_3$·7H$_2$O (0.025 g, 0.067 mmol) and dppmO$_2$ (0.112 g, 0.268 mmol) afforded colourless crystals of $[Ce(dppmO_2)_4]Cl_3$·4H$_2$O, by concentrating the ethanolic solution and layering with *n*-hexane (1 mL). Required for C$_{100}$H$_{100}$CeCl$_3$O$_{12}$P$_8$ (2020.1): C, 59.46; H, 4.99%. Found: C, 59.50; H, 4.50%. ^{1}H-NMR (CD$_2$Cl$_2$): δ = 1.52 (s, H$_2$O) 3.60 (vbr, [8H], PCH$_2$P), 7.10 (s, [32H], Ph), 7.35 (m, [16H], Ph), 7.70 (m, [32H], Ph). ^{31}P{^{1}H}-NMR (CD$_2$Cl$_2$): δ = 48.6 (s). IR (Nujol mull)/cm^{-1}: 3500 br, 1630 (H$_2$O), 1158, 1099s (P=O).

$[Pr(dppmO_2)_4]Cl_3$·6H$_2$O—To a solution of PrCl$_3$·6H$_2$O (0.025 g, 0.070 mmol) in ethanol (5 mL) was added a solution of dppmO$_2$ (0.117 g, 0.281 mmol) in ethanol (10 mL). A white powdered solid formed on slow evaporation of the ethanol. Required for C$_{100}$H$_{100}$Cl$_3$O$_{14}$P$_8$Pr (2020.9): C, 59.43; H, 4.99%. Found: C, 59.06; H, 4.62% ^{1}H-NMR (CD$_2$Cl$_2$): δ = 4.63 (m, [8H], PCH$_2$P), 7.19 (s, [32H], Ph), 7.44 (m, [16H], Ph), 8.19 (m, [32H], Ph). ^{31}P{^{1}H}-NMR (CD$_2$Cl$_2$): δ = 64.0 (s). IR (Nujol mull)/cm^{-1}: 3500 br, 1630 (H$_2$O), 1161, 1102 (P=O).

Table 1. X-ray crystallographic data [a].

Compound	[Ce(dppmO$_2$)$_4$] Cl$_3$·9EtOH	[Sm(dppmO$_2$)$_4$] Cl$_3$·9.5EtOH	[Gd(dppmO$_2$)$_4$] Cl$_3$·7EtOH	[Yb(dppmO$_2$)$_3$Cl] Cl$_2$·5EtOH	[Lu(dppmO$_2$)$_3$Cl] Cl$_2$·3.5CH$_2$Cl$_2$·10H$_2$O	[Lu(dppmO$_2$)$_2$Cl$_2$] Cl·CH$_2$Cl$_2$·0.5H$_2$O	[Yb(dppmO$_2$)$_3$(H$_2$O)] Cl$_3$·dppmO$_2$·12H$_2$O
Formula	C$_{118}$H$_{142}$CeCl$_3$O$_{17}$P$_8$	C$_{119}$H$_{145}$Cl$_3$O$_{17.5}$P$_8$Sm	C$_{114}$H$_{130}$Cl$_3$GdO$_{15}$P$_8$	C$_{87}$H$_{102}$Cl$_3$O$_{12}$P$_6$Yb$_1$	C$_{78.5}$H$_{93}$Cl$_{10}$LuO$_{16}$P$_6$	C$_{51}$H$_{47}$Cl$_5$LuO$_{4.5}$P$_4$	C$_{100}$H$_{114}$Cl$_3$O$_{21}$P$_8$Yb
M	2326.54	2359.80	2251.53	1805.010	2007.81	1208.49	2179.06
Crystal system	monoclinic	monoclinic	monoclinic	monoclinic	orthorhombic	orthorhombic	orthorhombic
Space group (no.)	P2/c (13)	P2/c (13)	P2/c (13)	Pc (7)	Pcca (54)	Pbca (61)	Pbca (61)
a/Å	29.5926(4	29.7348(4)	29.2352(5)	14.1964(2)	47.7209(4)	21.1303(3)	26.1035(2)
b/Å	23.2600(2)	23.1120(2)	23.1885(3)	12.9572(2)	12.7431(1)	21.7424(5)	27.6790(2)
c/Å	18.0187(2)	17.9915(3)	17.7500(3)	24.0141(3)	28.3698(2)	22.1612(3)	29.1187(2)
α/°	90	90	90	90	90	90	90
β/°	107.4810(10)	106.988(2)	107.116(2)	95.880(1)	90	90	90
γ/°	90	90	90	90	90	90	90
U/Å^3	11829.9(2)	11824.8(3)	11500.1(3)	4394.05(11)	17252.0(2)	10181.4(3)	21038.8(3)
Z	4	4	4	2	8	8	8
μ(Mo-K$_\alpha$)/mm^{-1}	0.613	0.724	0.817	1.322	1.629	2.372	1.153
F(000)	4340	4348	4676	1864	8184	4844	8984
Total number reflns	183494	181022	169524	66370	22287	75026	423866
R$_{int}$	0.0372	0.0393	0.0561	0.0354	0.0642	0.0558	0.0323
Unique reflns	30589	30564	24123	21530	22287	13145	27176
No. of params, restraints	1253, 132	1261, 35	1143, 0	849, 65	937,264	621, 5	1240, 1
R$_1$,wR$_2$ [I > 2σ(I)] [b]	0.0396, 0.0831	0.0371, 0.0788	0.0526, 0.1302	0.0346, 0.0798	0.0906, 0.1916	0.0337, 0.0708	0.0277, 0.0755
R$_1$, wR$_2$ (all data)	0.0516, 0.0870	0.0532, 0.0846	0.0650,0.1361	0.0387, 0.0814	0.0935, 0.1926	0.0552, 0.0774	0.0331, 0.0783

[a] common data: T = 100 K; wavelength (Mo-K$_\alpha$) = 0.71073 Å; θ(max) = 27.5°; [b] R$_1$ = Σ||Fo| − |Fc||/Σ|Fo|; wR$_2$ = [Σw(Fo^2 − Fc^2)^2/ΣwFo^4]$^{1/2}$.

[Nd(dppmO$_2$)$_4$]Cl$_3$·4H$_2$O—To a solution of NdCl$_3$·6H$_2$O (0.025 g, 0.070 mmol) in ethanol (5 mL) was added a solution of dppmO$_2$ (0.116 g, 0.279 mmol) in ethanol (10 mL). A white powdered solid formed on slow evaporation of the ethanol. Required for C$_{100}$H$_{96}$Cl$_3$NdO$_{12}$P$_8$ (1988.2): C, 60.41; H, 4.87%. Found: C, 60.41; H, 4.62%. ^{1}H-NMR (CD$_2$Cl$_2$): δ = 1.52 (s, H$_2$O) 3.66 (m, [8H], PCH$_2$P), 7.14 (s, [32H], Ph), 7.35 (m, [16H], Ph), 7.76 (m, [32H], Ph). ^{31}P{^{1}H}-NMR (CD$_2$Cl$_2$): δ = 62.9 (s). IR (Nujol mull)/cm^{-1}: 3500 br, 1630 (H$_2$O), 1159 s, 1101 s (P=O).

[Sm(dppmO$_2$)$_4$]Cl$_3$·4H$_2$O—To a solution of SmCl$_3$·6H$_2$O (0.025 g, 0.069 mmol) in ethanol (5 mL) was added a solution of dppmO$_2$ (0.114 g, 0.274 mmol) in ethanol (10 mL). Colourless crystals were formed via slow evaporation of the ethanol. Required for C$_{100}$H$_{96}$Cl$_3$O$_{12}$P$_8$Sm (1994.3): C, 60.22; H, 4.85%. Found: C, 60.05; H, 4.50%. ^{1}H-NMR (CD$_2$Cl$_2$): δ = 2.10 (s, H$_2$O), 5.08 (br, [8H], PCH$_2$P), 7.20 (s, [32H], Ph), 7.39 (m, [16H], Ph), 7.83 (m, [32H], Ph). ^{31}P{^{1}H}-NMR (CD$_2$Cl$_2$): δ = 35.6. IR (Nujol mull)/cm^{-1}: 3500 br, 1630 (H$_2$O), 1162 s, 1101 (P=O).

[Eu(dppmO$_2$)$_4$]Cl$_3$·4H$_2$O—To a solution of EuCl$_3$·6H$_2$O (0.025 g, 0.068 mmol) in ethanol (5 mL) was added a solution of dppmO$_2$ (0.114 g, 0.274 mmol) in ethanol (10 mL) and the solution was stirred for 20 min. The solution was then concentrated, and colourless crystals were formed through layering with *n*-hexane (1 mL). Required for C$_{100}$H$_{96}$Cl$_3$EuO$_{12}$P$_8$ (1995.9): C, 60.41; H, 4.87%. Found: C, 60.73; H, 4.71%. ^{1}H-NMR (CD$_2$Cl$_2$): δ = 2.15 (s, H$_2$O) 3.12 (br, [8H] PCH$_2$P), 7.18 (s, [32H], Ph), 7.38 (m, [16H], Ph), 7.83 (m, [32H], Ph). ^{31}P{^{1}H}-NMR (CD$_2$C$_2$): δ = 25.0 (br, "free" dppmO$_2$), −13.4. IR (Nujol mull)/cm^{-1}: 3500 br, 1630 (H$_2$O), 1159, 1099 (P=O).

[Gd(dppmO$_2$)$_4$]Cl$_3$·4H$_2$O—To a solution of GdCl$_3$·6H$_2$O (0.025 g, 0.067 mmol) in ethanol (5 mL) was added a solution of dppmO$_2$ (0.112 g, 0.269 mmol) in ethanol (10 mL). Colourless crystals were formed through slow evaporation of the solvent. Required for C$_{100}$H$_{96}$Cl$_3$GdO$_{12}$P$_8$ (2001.2): C, 60.02; H, 4.83%. Found: C, 60.05; H, 4.86%. ^{1}H-NMR (CD$_2$Cl$_2$): δ = no resonance. ^{31}P{^{1}H}-NMR (CD$_2$Cl$_2$): δ = no resonance. IR (Nujol mull)/cm^{-1}: 3500 br, 1630 (H$_2$O), 1160, 1099 (P=O).

[Sm(dppmO$_2$)$_3$Cl]Cl$_2$—To a solution of SmCl$_3$·6H$_2$O (0.025 g, 0.069 mmol) in ethanol (5 mL) was added a solution of dppmO$_2$ (0.086 g, 0.206 mmol) in ethanol (10 mL). The solvent was removed in vacuo and the resulting white solid was washed with cold ethanol. Colourless crystals were obtained via slow evaporation of an ethanolic solution of the product. Required for C$_{75}$H$_{66}$Cl$_3$O$_6$P$_6$Sm (1505.9): C, 59.80; H, 4.42%. Found: C, 59.62; H, 4.55%. ^{1}H-NMR (CD$_2$Cl$_2$): δ = 3.67 (br m, [6H], PCH$_2$P), 7.15 (br, [24H], Ph), 7.35 (m, [12H], Ph), 8.05 (m, [24H], Ph). ^{31}P{^{1}H}-NMR (CD$_2$Cl$_2$): δ = 38.15 (s). IR (Nujol mull)/cm^{-1}: 1153 s, 1097 s (P=O).

[Eu(dppmO$_2$)$_3$Cl]Cl$_2$—To a solution of EuCl$_3$·6H$_2$O (0.025 g, 0.068 mmol) in ethanol (5 mL) was added a solution of dppmO$_2$ (0.085 g, 0.205 mmol) in ethanol (10 mL). The solvent was removed in vacuo and the resulting white solid was washed with cold ethanol. Required for C$_{75}$H$_{66}$EuCl$_3$O$_6$P$_6$ (1507.49): C, 59.76; H, 4.41%. Found: C, 59.71; H, 4.56%. ^{1}H-NMR (CDCl$_3$): δ = 3.66 (br, [6H], PCH$_2$P), 7.03 (br m, [36H], Ph), 7.87 (br, [24H], Ph). ^{31}P{^{1}H}-NMR (CDCl$_3$): δ = −14.8 (s). IR (Nujol mull)/cm^{-1}: 1153 s, 1098 s (P=O).

[Gd(dppmO$_2$)$_3$Cl]Cl$_2$·3H$_2$O—To a solution of GdCl$_3$·6H$_2$O (0.025 g, 0.067 mmol) in ethanol (5 mL) was added a solution of dppmO$_2$ (0.084 g, 0.201 mmol) in ethanol (10 mL). The solvent was removed in vacuo and the resulting white solid was washed with cold ethanol. Required for C$_{75}$H$_{66}$Cl$_3$O$_6$P$_6$Gd (166.8): C, 57.49, H, 4.63%; Found: C, 57.17; H, 4.43%. ^{1}H-NMR (CD$_2$Cl$_2$): no resonance. ^{31}P{^{1}H}-NMR (CD$_2$Cl$_2$): no resonance. IR (Nujol mull)/cm^{-1}: 3500 br, 1630 (H$_2$O), 1155 s, 1098 s (P=O).

[Tb(dppmO$_2$)$_3$Cl]Cl$_2$·H$_2$O—To a solution of TbCl$_3$·6H$_2$O (0.025 g, 0.067 mmol) in ethanol (5 mL) was added a solution of dppmO$_2$ (0.084 g, 0.201 mmol) in ethanol (10 cm^3). The solvent was removed in vacuo and the resulting white solid was washed with cold ethanol. Required for C$_{75}$H$_{68}$Cl$_3$O$_7$P$_6$Tb (1532.5): C, 58.78; H, 4.47%. Found: C, 59.41; H, 4.54%. ^{1}H-NMR (CD$_2$Cl$_2$): δ = 1.9 (br H$_2$O), 3.50 (br m, [6H], PCH$_2$P), 5.89 (br, [36H], Ph), 7.46 (br, [24H], Ph). ^{31}P{^{1}H}-NMR (CD$_2$Cl$_2$): δ = −29.2 (s). IR (Nujol mull)/cm^{-1}: 3500 br, 1630 (H$_2$O), 1153 s, 1097 s (P=O).

[Dy(dppmO$_2$)$_3$Cl]Cl$_2$·H$_2$O—To a solution of TbCl$_3$·6H$_2$O (0.025 g, 0.066 mmol) in ethanol (5 mL) was added a solution of dppmO$_2$ (0.083 g, 0.199 mmol) in ethanol (10 cm^3). The solution was filtered

then concentrated and layered with hexane (1 mL) yielding a white powdered product. Colourless crystals were formed by layering a CH_2Cl_2 solution of the product with hexane. Required for $C_{75}H_{68}Cl_3DyO_7P_6$ (1536.0): C, 58.64; H, 4.46%. Found: C, 58.21; H, 4.63%. ^{1}H-NMR (CD_2Cl_2): $\delta = 1.9$ (vbr H_2O), 3.66 (br m, [6H], PCH$_2$P), 7.33 (br, [36H], Ph), 8.66 (br, [24H], Ph). ^{31}P{^{1}H}-NMR (CD_2Cl_2): $\delta = 18$ (vbr, s). IR (Nujol mull)/cm^{-1}: 3500 br, 1630 (H_2O), 1156 s, 1099 s (P=O).

[Ho(dppmO$_2$)$_3$Cl]Cl$_2$·H$_2$O—To a solution of HoCl$_3$ (0.050 g, 0.124 mmol) in ethanol (5 mL) was added a solution of dppmO$_2$ (0.230 g, 0.55 mmol) in ethanol (10 mL). The solvent was removed in vacuo and the resulting pale pink solid was washed with cold ethanol. Required for $C_{75}H_{68}Cl_3HoO_7P_6$ (1538.5): C, 58.66; H, 4.55%. Found: C, 59.41; H, 4.52%. ^{1}H-NMR (CD_2Cl_2): $\delta = 2.1$ (br, H_2O), 3.72 (br s, [6H], PCH$_2$P), 6.78 (br, [36H], Ph), 7.68 (br, [24H], Ph)]. ^{31}P{^{1}H}-NMR (CD_2Cl_2): $\delta = -13.5$ (s). IR (Nujol mull)/cm^{-1}: 3500 br, 1630 (H_2O), 1154 s, 1097 s (P=O).

[Er(dppmO$_2$)$_3$Cl]Cl$_2$·3H$_2$O—To a solution of ErCl$_3$·6H$_2$O (0.025 g, 0.065 mmol) in ethanol (5 mL) was added a solution of dppmO$_2$ (0.082 g, 0.196 mmol) in ethanol (10 mL). The solvent was removed in vacuo and the resulting white solid was washed with cold ethanol. Required for $C_{75}H_{72}Cl_3ErO_9P_6$ (1576.8): C, 57.13; H, 4.60%. Found: C, 57.08; H, 4.54%. ^{1}H-NMR (CD_2Cl_2): $\delta = \delta = 1.2$ (br, H_2O), 3.25 (br s, [6H], PCH$_2$P), 5.52 (vbr, [12H], Ph), 7.15 (br s, [24H], Ph)], 7.28 (br s, [24H], Ph)]. ^{31}P{^{1}H}-NMR (CD_2Cl_2): $\delta = -60.8$ (s). IR (Nujol mull)/cm^{-1}: 3500 br, 1630 (H_2O), 1155 s, 1097 s (P=O).

[Tm(dppmO$_2$)$_3$Cl]Cl$_2$·3H$_2$O—To a solution of TmCl$_3$·6H$_2$O (0.025 g, 0.065 mmol) in ethanol (5 mL) was added a solution of dppmO$_2$ (0.081 g, 0.195 mmol) in ethanol (10 mL). The solvent was removed in vacuo and the resulting white solid was washed with cold ethanol. Required for $C_{75}H_{72}Cl_3O_9P_6Tm$ (1578.5): C, 57.07; H, 4.60%. Found: C, 56.61; H, 4.45%. ^{1}H-NMR (CD_2Cl_2): $\delta = 3.48$ (m, [6H], PCH$_2$P), 7.11 (br, [24H], Ph), 7.68 (br, [36H], Ph)]. ^{31}P{^{1}H}-NMR (CD_2Cl_2): $\delta = -54.8$ (s). IR (Nujol mull)/cm^{-1}: 3500 br, 1630 (H_2O), 1156 s, 1096 s (P=O).

[Yb(dppmO$_2$)$_3$Cl]Cl$_2$·H$_2$O—To a solution of YbCl$_3$·6H$_2$O (0.025 g, 0.065 mmol) in ethanol (5 mL) was added a solution of dppmO$_2$ (0.080 g, 0.194 mmol) in ethanol (10 mL). The solvent was removed in vacuo and the resulting white powder was washed with cold ethanol. Required for $C_{75}H_{68}Cl_3O_7P_6Yb$ (1546.58): C, 58.24; H, 4.43%. Found: C, 58.73; H, 4.45%. ^{1}H-NMR (CD_2Cl_2): $\delta = 3.50$ (m, [6H], PCH$_2$P), 6.64 (br, [24H], Ph), 7.15 (br, [36H], Ph). ^{31}P{^{1}H}-NMR (CD_2Cl_2): $\delta = +9.2$ (s). IR (Nujol mull)/cm^{-1}: 3500 br, 1630 (H_2O), 1154 s, 1097 s (P=O).

3. Results

The reaction of LnCl$_3$·nH$_2$O (Ln = La [8], Ce, Pr, Nd, Sm, Eu or Gd; *n* = 6 or 7) with four mol. equivalents of dppmO$_2$ in ethanol gave good yields of tetrakis-dppmO$_2$ complexes, [Ln(dppmO$_2$)$_4$]Cl$_3$. The IR and ^{1}H-NMR spectra show the the isolated complexes retain significant amounts of lattice water, and sometimes EtOH, which is not removed by prolonged drying of the bulk powders in vacuo. The high molecular weights make the microanalyses rather insensitive to the amount of water, but are generally consistent with a formulation [Ln(dppmO$_2$)$_4$]Cl$_3$·nH$_2$O (*n* = 6: Ce, Pr; *n* = 4: Nd, Sm, Eu, Gd), although the amount of lattice solvent probably varies with the sample and is unlikely to be stoichiometric. The presence of significant amounts of lattice solvent is common in lanthanide phosphine oxide systems [7–10], and although evident in X-ray crystal structures, it is often disordered and difficult to model. Obtaining good quality crystals of the complexes proved difficult, but crystals of the Ce, Sm and Gd salts were obtained from various organic solvents and the compositions are shown in Table 1. The crystals contain different amounts of solvent of crystallisation to the bulk samples as they were grown from different media (and crystals were not dried in vacuo). The IR spectra (Table 2) show that the υ(PO) stretch in dppmO$_2$ at 1187 cm^{-1} has been lost and replaced by a new very strong and broad band ~1160 cm^{-1} and a second band at ~ 1100 cm^{-1}, which are due to the coordinated phosphine oxide groups. The frequencies appear invariant with the lanthanide present, which may be due to small differences being obscured by the width of the bands. In [LnCl$_3$(OPPh$_3$)$_3$] and [LnCl$_2$(OPPh$_3$)$_4$]$^+$ the frequency of the υ(PO) stretch increases by ~ 10 cm^{-1} between La and Lu [7]. The ^{31}P{^{1}H}-NMR chemical shift of dppmO$_2$ at $\delta = +25.3$ shows a high frequency shift to +33.1

in [La(dppmO$_2$)$_4$]Cl$_3$, whilst the corresponding spectra of the Ce, Pr, Nd and Sm complexes show larger shifts due to the presence of the paramagnetic lanthanide ion (Table 2). In contrast, although the solid [Eu(dppmO$_2$)$_4$]Cl$_3$ complex was isolated without difficulty, the ^{31}P{^{1}H}-NMR spectrum shows a strong feature at δ ~ +25 ("free" dppmO$_2$), along with a second resonance at δ = −13.4, which may be assigned to [Eu(dppmO$_2$)$_3$Cl]Cl$_2$ (see below), indicating substantial dissociation of one dppmO$_2$ in solution; the broad resonance of the free dppmO$_2$ is indicative of exchange on the NMR timescale. [Gd(dppmO$_2$)$_4$]Cl$_3$ was isolated, and its constitution confirmed by its X-ray crystal structure, but no ^{1}H or ^{31}P{^{1}H}-NMR resonances were observed, an effect seen in other gadolinium systems [6,7] and ascribed to fast relaxation by the f^7 configuration of the metal. Attempts to isolate [Ln(dppmO$_2$)$_4$]Cl$_3$ complexes for Ln = Dy-Lu were unsuccessful. We note that [Dy(dppmO$_2$)$_4$][CF$_3$SO$_3$]$_3$ [9] was isolated with triflate counter ions, but with chloride only [Dy(dppmO$_2$)$_3$Cl]Cl$_2$ was produced (below). An in situ ^{31}P{^{1}H}-NMR spectrum of CeCl$_3$·7H$_2$O + 2 dppmO$_2$ in CH$_2$Cl$_2$ showed a single resonance at δ = +48, which is consistent with formation of [Ce(dppmO$_2$)$_4$]$^{3+}$, confirming the preference for formation of the tetrakis complexes early in the series, even when there is a deficit of ligand.

Table 2. IR and ^{31}P{^{1}H}-NMR spectroscopic data.

| Complex	δ(^{31}P) [a]	υ(P=O) cm^{-1} [b]
dppmO$_2$	+25.3	1187
[La(dppmO$_2$)$_4$]Cl$_3$ [c]	+33.1	1159, 1100
[Ce(dppmO$_2$)$_4$]Cl$_3$	+48.6	1158, 1099
[Pr(dppmO$_2$)$_4$]Cl$_3$	+64.0	1161, 1102
[Nd(dppmO$_2$)$_4$]Cl$_3$	+62.9	1159, 1101
[Sm(dppmO$_2$)$_4$]Cl$_3$	+35.6	1162, 1101
[Eu(dppmO$_2$)$_4$]Cl$_3$	−13.4 (+25 dppmO$_2$)	1159, 1099
[Gd(dppmO$_2$)$_4$]Cl$_3$	Not observed	1160, 1099
[Sm(dppmO$_2$)$_3$Cl]Cl$_2$	+38.0	1153, 1097
[Eu(dppmO$_2$)$_3$Cl]Cl$_2$	−14.8	1153, 1098
[Gd(dppmO$_2$)$_3$Cl]Cl$_2$	Not observed	1155, 1099
[Tb(dppmO$_2$)$_3$Cl]Cl$_2$	−29.2	1153, 1097
[Dy(dppmO$_2$)$_3$Cl]Cl$_2$	+18.0	1156, 1099
[Ho(dppmO$_2$)$_3$Cl]Cl$_2$	−13.5	1154, 1095
[Er(dppmO$_2$)$_3$Cl]Cl$_2$	−60.75	1155, 1097
[Tm(dppmO$_2$)$_3$Cl]Cl$_2$	−54.8	1156, 1096
[Yb(dppmO$_2$)$_3$Cl]Cl$_2$	+9.2	1154, 1097
[Lu(dppmO$_2$)$_2$Cl$_2$]Cl [c]	+40.0	1158, 1098
[Lu(dppmO$_2$)$_3$Cl]Cl$_2$	+38.3	

[a] In CD$_2$Cl$_2$ solution 298 K; [b] Nujol mull; [c] Ref. [8].

The X-ray structures of [Ce(dppmO$_2$)$_4$]Cl$_3$ (Figure 1), [Sm(dppmO$_2$)$_4$]Cl$_3$ (Figure 2) and [Gd(dppmO$_2$)$_4$]Cl$_3$ (Figure 3) show distorted square antiprismatic cations, very similar to those in [La(dppmO$_2$)$_4$][PF$_6$]$_3$ [8] and [Nd(dppmO$_2$)$_4$]Cl$_3$ [15]. The average Ln-O distances in this series are: La = 2.514 Å, Ce = 2.486 Å, Nd = 2.465 Å, Sm = 2.429 Å and Gd = 2.420 Å, correlating well with the decreasing Ln^{3+} radii (La = 1.216 Å, Ce =1.196 Å, Nd = 1.163 Å, Sm = 1.132 Å, Gd = 1.107 Å). The P = O bond lengths and the O-Ln-O chelate angles do not vary significantly along the series. The Ce-O(P) distances in [Ce(dppmO$_2$)$_4$]Cl$_3$ are markedly longer than those in [Ce(Me$_3$PO)$_4$(H$_2$O)$_4$]Cl$_3$ (2.372(2)-2.423(2) Å) [16], which has a distorted dodecahedral geometry with a CeO$_8$ donor set.
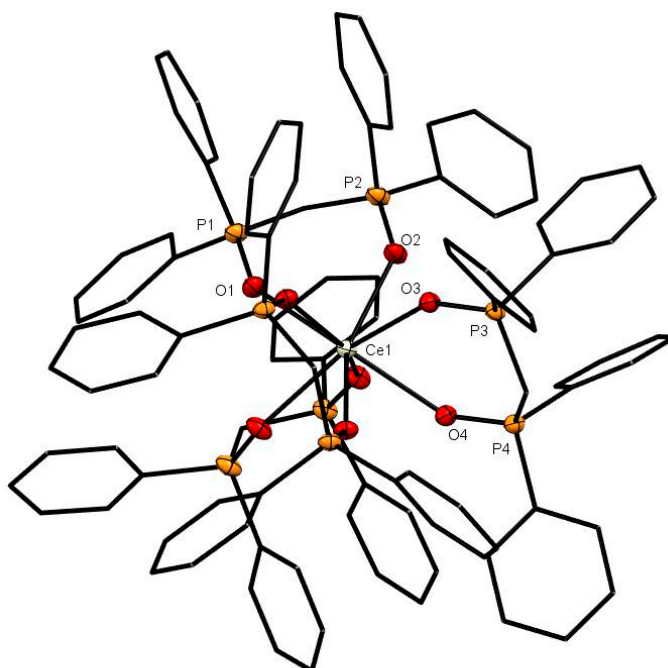
Figure 1. The cation in [Ce(dppmO$_2$)$_4$]Cl$_3$. The chloride anions and solvate molecules are omitted. Selected bond lengths (Å): Ce1–O1 = 2.4874(14), Ce1–O2 = 2.4790(14), Ce1–O3 = 2.4967(13), Ce1–O4 = 2.4803(14), P1–O1 = 1.5031(14), P2–O2 = 1.5021(14), P3–O3 = 1.5018(14), P4–O4 = 1.5031(14). Chelate angle O-Ce-O = 73.1° (av).
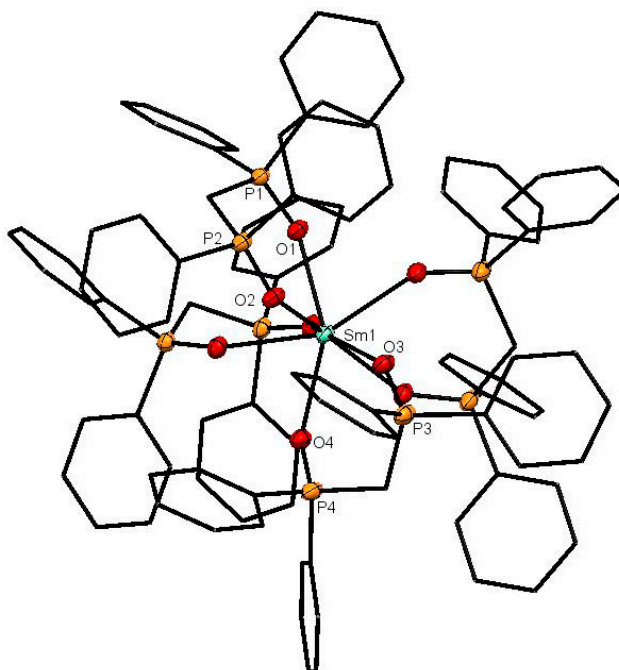

Figure 2. The cation in [Sm(dppmO$_2$)$_4$]Cl$_3$. The chloride anions and solvate molecules are omitted. Selected bond lengths (Å): Sm1–O1 = 2.4160(14), Sm1–O2 = 2.4400(15), Sm1–O3 = 2.4358(14), Sm1–O4 = 2.4268(15), P1–O1 = 1.5025(15), P2–O2 = 1.5019(15), P3–O3 = 1.4961(15), P4–O4 = 1.4961(16). Chelate angle O-Sm-O = 72.9° (av).
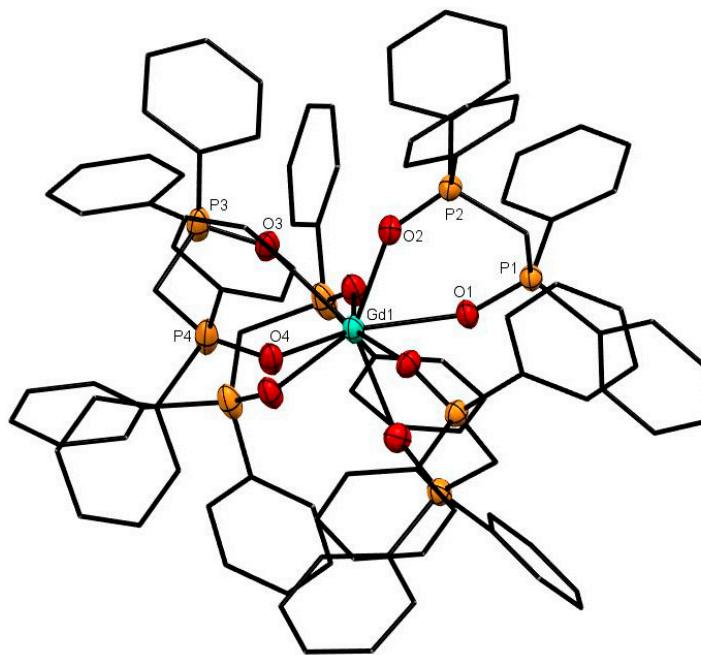
Figure 3. The cation in [Gd(dppmO$_2$)$_4$]Cl$_3$. The chloride anions and solvate molecules are omitted. Selected bond lengths (Å): Gd1–O1 = 2.420(2), Gd1–O2 = 2.409(3), Gd1–O3 = 2.415(2), Gd1–O4 = 2.398(2), P1–O1 = 1.504(2), P2–O2 = 1.501(3), P3–O3 = 1.501(3), P4–O4 = 1.501(3). Chelate angle O-Sm-O = 73.1° (av).

The reaction of LnCl$_3$·6H$_2$O (Ln =Sm, Eu, Gd, Tb, Dy, Ho, Er, Tm, Yb) with 3 mol. equivalents of dppmO$_2$ in EtOH, followed by concentration of the solution or precipitation with hexane, afforded [Ln(dppmO$_2$)$_3$Cl]Cl$_2$ complexes. Examination of the IR and ^{1}H-NMR spectra indicated these incorporated less water or ethanol lattice solvent molecules than the [Ln(dppmO$_2$)$_4$]Cl$_3$, and this was confirmed by the microanalyses. The Sm and Eu complexes appear largely free of solvent of crystallisation, whilst the Tb, Ho and Yb approximate to [Ln(dppmO$_2$)$_3$Cl]Cl$_2$·H$_2$O, and the Gd, Er and Tm complexes are [Ln(dppmO$_2$)$_3$Cl]Cl$_2$·3H$_2$O; again, this is likely to vary from sample to sample and with the isolation method. The IR spectra (Table 2) show the two υ(PO) bands as in the tetrakis complexes, but the higher energy bands of the tris complexes are ~ 5–10 cm^{-1} lower in frequency than in the former. We were unable to identify υ(Ln-Cl) vibrations in the far IR spectra. The ^{31}P{^{1}H}-NMR spectra of the [Ln(dppmO$_2$)$_3$Cl]Cl$_2$ show single resonances to high or low frequency of dppmO$_2$ depending on the f^n configuration of the Ln ion present (Table 2) and are generally similar to those found in other systems [5–7], although the magnitude of the shifts varies widely with the specific f^n configuration. The line broadening is also highly variable between complexes of different Ln ions. The addition of dppmO$_2$ to a solution of [Ln(dppmO$_2$)$_3$Cl]Cl$_2$ (Ln = Eu, Gd, Tb, Dy, Ho, Er, Tm, Yb) in CH$_2$Cl$_2$ showed ^{31}P{^{1}H}-NMR resonances assignable to "free" dppmO$_2$ and [Ln(dppmO$_2$)$_3$Cl]Cl$_2$, but no new resonances that could be attributed to the formation of significant amounts of [Ln(dppmO$_2$)$_4$]$^{3+}$. Although the resonances are broad in some cases, the observed chemical shifts are identical to those in pure [Ln(dppmO$_2$)$_3$Cl]Cl$_2$. For [Sm(dppmO$_2$)$_3$Cl]Cl$_2$ δ(^{31}P{^{1}H}) = 38, the resonance shifts to δ = 35.6 upon addition of dppmO$_2$, attributable to the formation of [Sm(dppmO$_2$)$_4$]Cl$_3$, showing that both tris- and tetrakis-dppmO$_2$ complexes exist in solution for samarium in the presence of the appropriate amount of ligand.

The X-ray structures of [Er(dppmO$_2$)$_3$Cl]Cl$_2$ (Er-O = 2.28 Å av.) [17], [Yb(dppmO$_2$)$_3$Cl]Cl$_2$ (Figure 4; Yb-O = 2.28 Å av.) and [Dy(dppmO$_2$)$_3$Cl]Cl$_2$ (Figure S43) show pentagonal bipyramidal cations with an apical chloride. The Ln-O distances are rather variable (Er-O = 2.244(6)–2.328(6) Å; Yb-O = 2.250(2)–2.269(3) Å), but are shorter than those in the tetrakis-dppmO$_2$ cations, reflecting both the reduced coordination number and the smaller metal ion radii (Er = 1.062, Yb = 1.042 Å). The contraction in ionic radii is also evident in the Ln-Cl distances of 2.598(2) Å (Er) and 2.5829(9) Å (Yb). Crystals

of [Dy(dppmO$_2$)$_3$Cl]Cl$_2$ were also obtained and show the same cation type, but during refinement, several of the phenyl rings exhibited severe disorder and the data are therefore not included here (Figure S43).
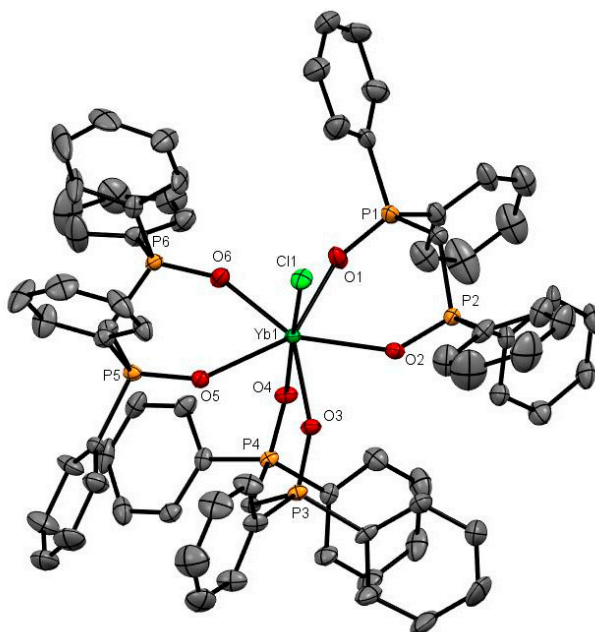

Figure 4. The X-ray structure of [Yb(dppmO$_2$)$_3$Cl]Cl$_2$. The chloride anions and solvate molecules are omitted. Selected bond lengths (Å) and angles (°): Yb1–Cl1 = 2.5834(9), Yb1–O1 = 2.298(3), Yb1–O2 = 2.282(3), Yb1–O3 = 2.250(2), Yb1–O4 = 2.248(2), Yb1–O5 = 2.338(2), Yb1–O6 = 2.269(3), P–O = 1.494(3)-1.509(3), Cl1–Yb1–O4 = 173.89(9), O1–Yb1–O2 = 73.79(9), O3–Yb1–O4 = 80.64(9), O5–Yb1–O6 = 73.95(9).

Lutetium was previously reported to form the only bis-dppmO$_2$ complex, [Lu(dppmO$_2$)$_2$Cl$_2$]Cl, in this series [8], and this has now been confirmed by the X-ray crystal structure which shows a *cis*-octahedral geometry (Figure 5). The Lu-O distance of 2.230 Å (av) is shorter than the Ln-O distances in the seven- or eigth-coordinate complexes, and correlates both with the reduced coordination number and the smaller radius of Lu^{3+} (1.032 Å). Treatment of a CH$_2$Cl$_2$ solution of [Lu(dppmO$_2$)$_2$Cl$_2$]Cl with dppmO$_2$ caused the ^{31}P{^{1}H}-NMR resonance to shift from +40 to +38.3, which suggests that [Lu(dppmO$_2$)$_3$Cl]Cl$_2$ forms in solution. A few crystals of this product were isolated from a mixture containing excess dppmO$_2$. These showed a pentagonal bipyramidal dication (Figure 6). As expected, the Lu-Cl and Lu-O bond lengths are slightly longer than in the six-coordinate cation, but are shorter than the corresponding bonds in [Yb(dppmO$_2$)$_3$Cl]Cl$_2$, showing that the expected contraction continues along the series. The complex, [Lu(dppmO$_2$)$_3$(H$_2$O)][CF$_3$SO$_3$]$_3$, is known and its X-ray crystal structure showed seven-coordinate lutetium [11]. Although not confirmed by an X-ray structure, yttrium is reported to form a six-coordinate complex, [Y(dppmO$_2$)$_2$Cl$_2$]Cl [18].

A different crystal isolated from the YbCl$_3$-dppmO$_2$ reaction proved, on structure solution, to be [Yb(dppmO$_2$)$_3$(H$_2$O)]Cl$_3$·dppmO$_2$·12H$_2$O (Figure 7), which contains a seven-coordinate Yb centre coordinated to three dppmO$_2$ and a water molecule, with the Lu-coordinated water hydrogen-bonded to an adjacent uncoordinated dppmO$_2$ molecule. The geometry is best described as a very distorted pentagonal bipyramid with the water occupying an equatorial position and is similar to the geometry found in [Lu(dppmO$_2$)$_3$(H$_2$O)][CF$_3$SO$_3$]$_3$ [11]. The Yb-OH$_2$ distance of 2.3263(14) Å is ~ 0.05 Å longer than the Yb-O(P).

A large number of disordered solvate water molecules were also present, which proved very difficult to model, but the geometry of the ytterbium cation is clearly defined.
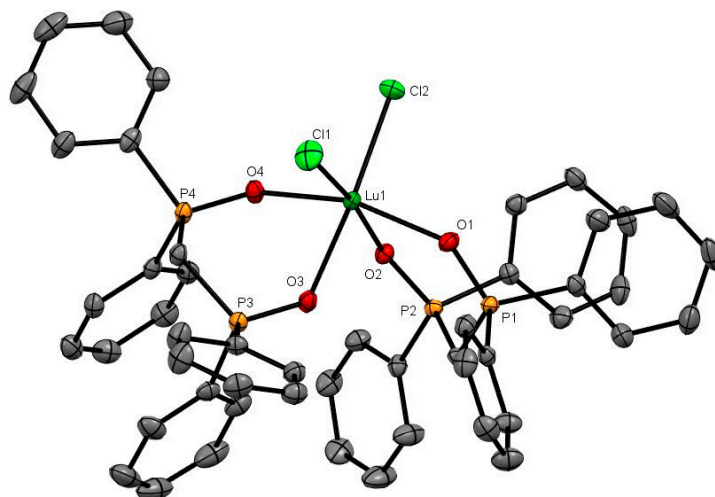
Figure 5. The cation in [Lu(dppmO$_2$)$_2$Cl$_2$]Cl. Selected bond lengths (Å) and angles (°): Lu1–Cl1 = 2.5581(8), Lu1–Cl2 = 2.5163(7), Lu1–O1 = 2.227(2), Lu1–O2 = 2.227(2), Lu1–O3 = 2.274(2), Lu1–O4 = 2.200(2), P1–O1 = 1.510(2), P2–O2 = 1.506(2), P3–O3 = 1.513(2), P4–O4 = 1.507(2), Cl2–Lu1–Cl1 = 95.97(3), O1–Lu1–Cl1 = 97.27(6), O1–Lu1–Cl2 = 99.68(6), O1–Lu1–O2 = 81.56(8), O1–Lu1–O3 = 85.65(7), O2–Lu1–Cl2 = 91.94(5), O2–Lu1–O3 = 84.89(7), O3–Lu1–Cl1 = 87.22(6), O4–Lu1–Cl1 = 94.66(6), O4–Lu1–Cl2 = 92.55(6), O4–Lu1–O2 = 84.74(8), O4–Lu1–O3 = 81.36(7).
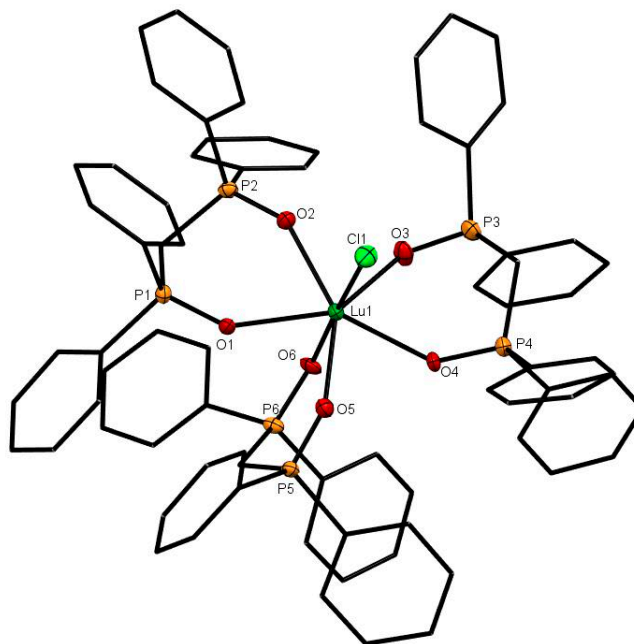
Figure 6. The X-ray structure of [Lu(dppmO$_2$)$_3$Cl]Cl$_2$. The chloride anions and solvate molecules are omitted. Selected bond lengths (Å) and angles (°): Lu1–Cl1 = 2.5604(7), Lu1–O1 = 2.341(5), Lu1–O2 = 2.268(5), Lu1–O3 = 2.268(5), Lu1–O4 = 2.297(5), Lu1–O5 = 2.354(5), Lu1–O6 = 2.227(5), P–O = 1.497(5)-1.510(5), Cl1–Lu1–O6 = 176.35(14), O1–Lu1–O2 = 73.37(17), O3–Lu1–O4 = 73.37(17), O5–Lu1–O6 = 83.45(18).
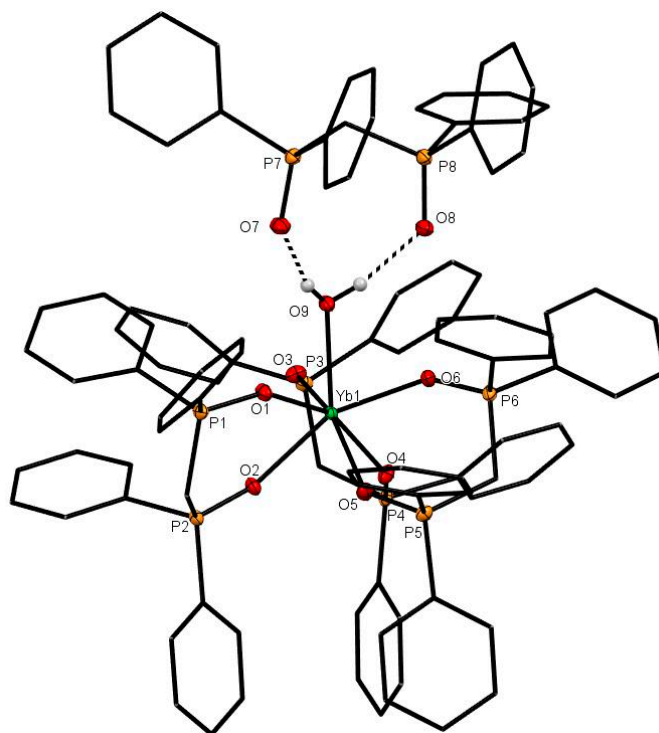
Figure 7. The cation in [Yb(dppmO$_2$)$_3$(H$_2$O)]Cl$_3$·dppmO$_2$·12H$_2$O also showing the hydrogen-bonded dppmO$_2$ molecule. Selected bond lengths (Å): Yb1–O3 = 2.2341(14), Yb1–O2 = 2.2899(13), Yb1–O9 = 2.3263(14), Yb1–O4 = 2.2683(13), Yb1–O6 = 2.2208(13), Yb1–O1 = 2.2328(13), Yb1–O5 = 2.2696(14), P$_n$–O$_n$ (n = 1–6) = 1.5034(14)–1.5072(14), P7–O7 = 1.4924(15), P8–O8 = 1.4926(15).

4. Discussion

The chemistry of dppmO$_2$ with lanthanides described in the previous section proves to be very systematic along the series La–Lu. For La–Gd, it was possible to isolate [Ln(dppmO$_2$)$_4$]Cl$_3$. Although it could be isolated in the solid state, the solution ^{31}P-NMR spectroscopic data indicate that [Eu(dppmO$_2$)$_4$]Cl$_3$ was largely dissociated in CH$_2$Cl$_2$ solution into [Eu(dppmO$_2$)$_3$Cl]$^{2+}$ and dppmO$_2$; the isolation of the tetrakis-dppmO$_2$ complex no doubt resulting from it being the least soluble species in an exchanging mixture in solution, although present in very minor amounts. The case of [Gd(dppmO$_2$)$_4$]Cl$_3$ is likely to be similar, although the fast relaxation of the f^7 ion precluded ^{31}P-NMR study. For the elements Sm-Yb, the complexes [Ln(dppmO$_2$)$_3$Cl]Cl$_2$ were readily isolated, but only for samarium was it possible to convert [Ln(dppmO$_2$)$_3$Cl]Cl$_2$ to [Ln(dppmO$_2$)$_4$]Cl$_3$ in CH$_2$Cl$_2$ solution by treatment with more dppmO$_2$. Similarly, at the end of the series, the complex isolated was [Lu(dppmO$_2$)$_2$Cl$_2$]Cl, for which treatment with dppmO$_2$ afforded a new species in solution, identified as [Lu(dppmO$_2$)$_3$Cl]Cl$_2$ by a structure determination from a few crystals obtained in the presence of excess dppmO$_2$, although a bulk sample could not be isolated [8]. The change from eight-coordination in [Ln(dppmO$_2$)$_4$]Cl$_3$ at the beginning of the series, to seven-coordination from Sm onwards, and finally to six-coordination at Lu, parallels the reduction in Ln^{3+} radii. Isolation of both the eight- and seven-coordinate complexes was possible only for Sm, Eu and Gd. However, one should note that the chloride counter ions also have some role, in that whilst in the LnCl$_3$/dppmO$_2$ series tetrakis-dppmO$_2$ species did not form beyond Gd, the complex [Dy(dppmO$_2$)$_4$][CF$_3$SO$_3$]$_3$ [9] has been isolated from dmf solution with triflate counter ions. The role that anions and solvents play in lanthanide chemistry is often overlooked [2], but can be critical in determining which complex is isolated from solution. For example, the reaction of LnCl$_3$ with Ph$_3$PO results in isolation of [Ln(Ph$_3$PO)$_3$Cl$_3$] from acetone, but [Ln(Ph$_3$PO)$_4$Cl$_2$]Cl from ethanol [7]. On further examination by ^{31}P-NMR spectroscopy, both species were found to be present in either solvent (in varying amounts), and the form isolated

reflected the least soluble complex in the particular solvent, which then precipitated from the mixture of rapidly interconverting species.

5. Conclusions

Through this synthetic, structural and spectroscopic study of the coordination of dppmO$_2$ to the lanthanide trichlorides, we have established where the switch from eight-, to seven-, to six-coordination at the Ln(III) centre occurs along the lanthanide series, with X-ray crystallographic authentication for representative examples. The data also reveal subtle, but systematic, variations in the spectroscopic (e.g., ν(PO)) and structural parameters across the series, reflecting the change in ionic radii, the charge:radius ratio and also the influence of the presence of the competitive chloride ions.

Supplementary Materials: The following are available online at http://www.mdpi.com/2624-8549/2/4/60/s1; Figure S1–^{1}H-NMR spectrum of [Ce(dppmO$_2$)$_4$]Cl$_3$ in CD$_2$Cl$_2$; Figure S2–^{31}P{^{1}H} spectrum of Ce(dppmO$_2$)$_4$]Cl$_3$ in CD$_2$Cl$_2$; Figure S3–Infrared spectrum of [Ce(dppmO$_2$)$_4$]Cl$_3$ (Nujol mull); Figure S4–^{1}H-NMR spectrum of [Pr(dppmO$_2$)$_4$]Cl$_3$ in CD$_2$Cl$_2$; Figure S5–^{31}P{^{1}H}-NMR spectrum of [Pr(dppmO$_2$)$_4$]Cl$_3$ in CD$_2$Cl$_2$; Figure S6–Infrared spectrum of [Pr(dppmO$_2$)$_4$]Cl$_3$ (Nujol mull); Figure S7–^{1}H-NMR spectrum of [Nd(dppmO$_2$)$_4$]Cl$_3$ in CD$_2$Cl$_2$; Figure S8–^{31}P{^{1}H}-NMR spectrum of [Nd(dppmO$_2$)$_4$]Cl$_3$ in CD$_2$Cl$_2$; Figure S9—Infrared spectrum of [Nd(dppmO$_2$)$_4$]Cl$_3$ (Nujol mull); Figure S10–^{1}H-NMR spectrum of [Sm(dppmO$_2$)$_4$]Cl$_3$ in CD$_2$Cl$_2$; Figure S11—^{31}P{^{1}H}-NMR spectrum of [Sm(dppmO$_2$)$_4$]Cl$_3$ in CD$_2$Cl$_2$; Figure S12—Infrared spectrum of [Sm(dppmO$_2$)$_4$]Cl$_3$ (Nujol mull); Figure S13–^{1}H-NMR spectrum of [Eu(dppmO$_2$)$_4$]Cl$_3$ in CD$_2$Cl$_2$; Figure S14—^{31}P{^{1}H}-NMR spectrum of [Eu(dppmO$_2$)$_4$]Cl$_3$ in CD$_2$Cl$_2$; Figure S15—Infrared spectrum of [Eu(dppmO$_2$)$_4$]Cl$_3$ (Nujol mull); Figure S16—Infrared spectrum of [Gd(dppmO$_2$)$_4$]Cl$_3$ (Nujol mull); Figure S17—^{1}H-NMR spectrum of [SmCl(dppmO$_2$)$_3$]Cl$_2$ in CD$_2$Cl$_2$ (* = EtOH); Figure S18—^{31}P{^{1}H}-NMR spectrum of [SmCl(dppmO$_2$)$_3$]Cl$_2$ in CD$_2$Cl$_2$; Figure S19—Infrared spectrum of [SmCl(dppmO$_2$)$_3$]Cl$_2$ (Nujol mull); Figure S20—^{1}H-NMR spectrum of [EuCl(dppmO$_2$)$_3$]Cl$_2$ in CDCl$_3$; Figure S21—^{31}P{^{1}H}-NMR spectrum of [EuCl(dppmO$_2$)$_3$]Cl$_2$ in CDCl$_3$; Figure S22—^{31}P{^{1}H}-NMR spectrum of [EuCl(dppmO$_2$)$_3$]Cl$_2$ + excess dppmO$_2$ in CDCl$_3$; Figure S23—Infrared spectrum of [EuCl(dppmO$_2$)$_3$]Cl$_2$ (Nujol mull); Figure S24—Infrared spectrum of [GdCl(dppmO$_2$)$_3$]Cl$_2$ (Nujol mull); Figure S25—^{1}H-NMR spectrum of [TbCl(dppmO$_2$)$_3$]Cl$_2$ in CD$_2$Cl$_2$ (* = EtOH); Figure S26—^{31}P{^{1}H}-NMR spectrum of [TbCl(dppmO$_2$)$_3$]Cl$_2$ in CD$_2$Cl$_2$; Figure S27—Infrared spectrum of [TbCl(dppmO$_2$)$_3$]Cl$_2$ (Nujol mull); Figure S28—^{1}H-NMR spectrum of [DyCl(dppmO$_2$)$_3$]Cl$_2$ in CD$_2$Cl$_2$; Figure S29—^{31}P{^{1}H}-NMR spectrum of [DyCl(dppmO$_2$)$_3$]Cl$_2$ in CD$_2$Cl$_2$; Figure S30—Infrared spectrum of [DyCl(dppmO$_2$)$_3$]Cl$_2$ (Nujol mull); Figure S31—^{1}H-NMR spectrum of [HoCl(dppmO$_2$)$_3$]Cl$_2$ in CD$_2$Cl$_2$ (* = EtOH); Figure S32—^{31}P{^{1}H}-NMR spectrum of [HoCl(dppmO$_2$)$_3$]Cl$_2$ in CD$_2$Cl$_2$; Figure S33—Infrared spectrum of [HoCl(dppmO$_2$)$_3$]Cl$_2$ (Nujol mull); Figure S34—^{1}H-NMR spectrum of [ErCl(dppmO$_2$)$_3$]Cl$_2$ in CD$_2$Cl$_2$ (* = EtOH); Figure S35—^{31}P{^{1}H}-NMR spectrum of [ErCl(dppmO$_2$)$_3$]Cl$_2$ in CD$_2$Cl$_2$; Figure S36—Infrared spectrum of [ErCl(dppmO$_2$)$_3$]Cl$_2$ (Nujol mull); Figure S37—^{1}H-NMR spectrum of [TmCl(dppmO$_2$)$_3$]Cl$_2$ in CD$_2$Cl$_2$ (* = EtOH); Figure S38—^{31}P{^{1}H}-NMR spectrum of [TmCl(dppmO$_2$)$_3$]Cl$_2$ in CD$_2$Cl$_2$; Figure S39—Infrared spectrum of [TmCl(dppmO$_2$)$_3$]Cl$_2$ (Nujol mull); Figure S40—^{1}H-NMR spectrum of [YbCl(dppmO$_2$)$_3$]Cl$_2$ in CD$_2$Cl$_2$ (* = EtOH); Figure S41—^{31}P{^{1}H}-NMR spectrum of [YbCl(dppmO$_2$)$_3$]Cl$_2$ in CD$_2$Cl$_2$; Figure S42—Infrared spectrum of [YbCl(dppmO$_2$)$_3$]Cl$_2$ (Nujol mull); Figure S43—The cation in [DyCl(dppmO$_2$)$_3$]Cl$_2$. The chloride anions and solvate molecules are omitted.

Author Contributions: Conceptualization, R.D.B., W.L. and G.R.; formal analysis, R.D.B.; investigation, R.D.B.; data curation, R.D.B.; writing—original draft preparation, R.D.B. and W.L.; writing—review and editing, R.D.B., W.L. and G.R.; supervision, W.L. and G.R. All authors have read and agreed to the published version of the manuscript.

Conflicts of Interest: The authors declare no conflict of interest.

References

1. Cotton, S.A. *Lanthanide and Actinide Chemistry*; John Wiley: Chichester, UK, 2006.
2. Cotton, S.A.; Raithby, P.R. Systematics and surprises in lanthanide coordination chemistry. *Coord. Chem. Rev.* **2017**, *340*, 220–231. [CrossRef]
3. Platt, A.W.G. Lanthanide phosphine oxide complexes. *Coord. Chem. Rev.* **2017**, *340*, 62–78. [CrossRef]
4. Lees, A.M.J.; Platt, A.W.G. Complexes of lanthanide nitrates with bis(diphenylphosphino)methane dioxide. *Inorg. Chem.* **2003**, *42*, 4673–4679. [CrossRef] [PubMed]

5. Levason, W.; Newman, E.H.; Webster, M. Tetrakis(triphenylphosphine oxide) complexes of the lanthanide nitrates; synthesis, characterization and crystal structures of [La(Ph$_3$PO)$_4$(NO$_3$)$_3$] and [Lu(Ph$_3$PO)$_4$(NO$_3$)$_2$]NO$_3$. *Polyhedron* **2000**, *19*, 2697–2705. [CrossRef]
6. Hill, N.J.; Leung, L.-S.; Levason, W.; Webster, M. Homoleptic octahedral hexakis(trimethylphosphine oxide)lanthanide hexafluorophosphates, [Ln(Me$_3$PO)$_6$][PF$_6$]$_3$; synthesis, structures and properties. *Inorg. Chim. Acta* **2003**, *343*, 169–174. [CrossRef]
7. Glazier, M.J.; Levason, W.; Matthews, M.L.; Thornton, P.L.; Webster, M. Synthesis, properties and solution speciation of lanthanide chloride complexes of triphenylphosphine oxide. *Inorg. Chim. Acta* **2004**, *357*, 1083–1091. [CrossRef]
8. Bannister, R.D.; Levason, W.; Reid, G. Diphosphine dioxide complexes of lanthanum and lutetium—The effects of ligand architecture and counter-anion. *Polyhedron* **2017**, *133*, 264–269. [CrossRef]
9. Jin, Q.-H.; Wu, J.-Q.; Zhang, Y.-Y.; Zhang, C.-L. Crystal structure of tetra(bis(diphenylphosphino)methane dioxide-*O,O*]dysprosium(III) tri(trifluoromethanesulfonate)-N,N-dimethylformamide (1:2) [Dy(C$_{25}$H$_{22}$P$_2$O$_2$)$_4$] [CF$_3$SO$_3$]$_3$ ·2C$_3$H$_7$NO. *Z. Krystallogr. NCS* **2009**, *224*, 428–432. [CrossRef]
10. Huang, L.; Ma, B.-Q.; Huang, C.-H.; Makk, T.C.W.; Yao, G.-Q.; Xu, G.-X. Synthesis, characterisayion and crystal structure of a complex of europium perchlorate with methylenebis(diphenylphosphine oxide). *J. Coord. Chem.* **2001**, *54*, 95–103. [CrossRef]
11. Fawcett, J.; Platt, A.W.G. Structures and catalytic properties of complexes of bis(diphenylphosphino)methane dioxide with scandium and lanthanide trifluoromethanesulfonates. *Polyhedron* **2003**, *22*, 967–973. [CrossRef]
12. Levason, W.; Patel, R.; Reid, G. Catalytic air oxidation of tertiary phosphines in the presence of tin(IV) iodide. *J. Organomet. Chem.* **2003**, *688*, 280–282. [CrossRef]
13. Sheldrick, G.M. A short history of SHELX. *Acta Crystallog. Sect. A* **2008**, *64*, 112–122. [CrossRef] [PubMed]
14. Sheldrick, G.M. Crystal structure refinement with SHELX. *Acta Crystallog. Sect. C* **2015**, *71*, 3–8. [CrossRef] [PubMed]
15. Grachova, E.V.; Linti, G.; Vologzhanina, A.V. *Personal communication CCDC 860683: Experimental Crystal Structure Determination*; The Cambridge Crystallographic Data Centre (CCDC): Cambridge, UK, 2016. [CrossRef]
16. Hill, N.J.; Leung, L.-S.; Levason, W.; Webster, M. Tetraaquatetrakis(trimethylphosphineoxide-κ-O)cerium(III) trichloride trihydrate. *Acta Crystallog. Sect. C* **2002**, *58*, m295. [CrossRef] [PubMed]
17. Grachova, E.V.; Linti, G.; Vologzhanina, A.V. *Personal communication CCDC 860682: Experimental Crystal Structure Determination*; The Cambridge Crystallographic Data Centre (CCDC): Cambridge, UK, 2016. [CrossRef]
18. Hill, N.J.; Levason, W.; Popham, M.C.; Reid, G.; Webster, M. Yttrium halide complexes of phosphine- and arsine-oxides: Synthesis, multinuclear NMR and structural studies. *Polyhedron* **2002**, *21*, 445–455. [CrossRef]